

# Impact of Irradiation Side on Muon-Induced Single Event Upsets in 65-nm Bulk SRAMs

Yifan Deng, Yukinobu Watanabe, Seiya Manabe, Wang Liao, *Member, IEEE*, Masanori Hashimoto, *Senior Member, IEEE*, Shin-Ichiro Abe, Motonobu Tampo, and Yasuhiro Miyake

**Abstract**—We have newly analyzed negative and positive muon-induced single event upset (SEU) data in irradiation tests from the package side (PS) of 65-nm bulk static random access memory (SRAM) and compared with previous results of irradiation tests from the board side (BS). The peak SEU cross section is at 28 MeV/c for PS irradiation, which differs from 38 MeV/c for BS irradiation. The magnitude of the peak SEU cross section for PS irradiation is approximately twice that of BS irradiation for both positive and negative muons. Through simulations using Geant4, we explain the difference quantitatively. This simulation also reproduces the experimental SEU cross sections for tilted incidence of the muon beam onto the device board. The soft error rates (SERs) are estimated under a realistic environment considering the zenith angle distribution of muon flux. As a result, it was found that the estimated SERs were not significantly different from the case without zenith angle distribution. This result indicates that experimental data from irradiation tests in which the device board is placed perpendicular to the incident beam are expected to be useful for estimating muon-induced SERs in terrestrial environments.

**Index Terms**—Single event upset, Soft error rate, SRAMs, Negative and positive muons, Irradiation side, Accelerated testing, Monte Carlo simulation, Geant4

## I. INTRODUCTION

TERRESTRIAL radiation can threaten the safety of memory and logic units in integrated circuits by Single Event Upsets (SEUs). Cosmic-ray neutrons have always been a main

Manuscript submitted October 23rd, 2023. This work was supported by Grant-in-Aid for Scientific Research (S) from the Japan Society for the Promotion of Science under Grant 19H05664.

Y. Deng is with the Interdisciplinary Graduate School of Engineering Sciences, Kyushu University, Fukuoka 816-8580, Japan. (e-mail: deng.yifan.462@s.kyushu-u.ac.jp).

Y. Watanabe is with the Faculty of Engineering Sciences, Kyushu University, Fukuoka 816-8580, Japan (e-mail: watanabe@aes.kyushu-u.ac.jp).

S. Manabe was with the Interdisciplinary Graduate School of Engineering Sciences, Kyushu University, Fukuoka 816-8580, Japan, and is currently with the Research Institute for Measurement and Analytical Instrumentation (RIMA), National Institute of Advanced Industrial Science and Technology, Ibaraki 305-8568, Japan. (e-mail: s-manabe@aist.go.jp)

W. Liao is with the School of System Engineering, Kochi University of Technology, Kochi 782-8502, Japan (e-mail: liao.wang@kochi-tech.ac.jp).

M. Hashimoto is with the Graduate School of Informatics, Kyoto University, Kyoto 606-8501, Japan. (e-mail: hashimoto@i.kyoto-u.ac.jp).

S.-I. Abe is with the Research Group for Radiation Transport Analysis, Japan Atomic Energy Agency, Ibaraki, 319-1184, Japan (e-mail: abe.shinichiro@jaea.go.jp).

M. Tampo is with the Muon Science Laboratory, High Energy Accelerator Research Organization (KEK), Tsukuba 319-1106, Japan (e-mail: mtampo@post.kek.jp).

Y. Miyake is with the Muon Science Laboratory, High Energy Accelerator Research Organization (KEK), Tsukuba 319-1106, Japan, and with the Materials and Life Science Division, Japan Proton Accelerator Research Complex Center, Muon Section, Ibaraki 319-1195, Japan (e-mail: ymiyake@post.kek.jp).

radiation source for SEUs in terrestrial environments. With the miniaturization of semiconductor devices and the decrease in operating voltage, a growing interest in whether cosmic muons may be another source of SEUs. A number of experimental and simulation works on muons induced SEU cross section, and Soft Error Rate (SER) predictions were performed [1]–[10].

In the previous study [6], negative and positive muon acceleration tests were performed for 65-nm bulk SRAMs at the Muon Science Facility (MUSE) in the Materials and Life Science Experimental Facility (MLF), Japan Proton Accelerator Research Complex (J-PARC) [11], [12]. In the experiment period, both tests of package side (PS) irradiation and board side (BS) irradiation were done, while the results of PS irradiation have not been published. However, the SEU cross-sections and the SER predictions from acceleration tests highly depend on the experimental conditions. It was reported that the irradiation side impacts neutron-induced SEUs due to the different atomic composition of the material in the package and PCB board [13].

Since muons pass through different thicknesses and materials before reaching the Sensitive Volume (SV) in cases of varying irradiation sides, we are also interested in the impact of the irradiation side on muon-induced SEUs. Thus, we re-analyzed the results of tests with different irradiation sides, i.e., PS and BS, to study the impact of the irradiation side on muon induced SEU on 65-nm Bulk SRAMs. Then we analyzed and investigated how different incident depths due to different irradiation sides affect positive and negative muon induced SEU cross sections based on the test results and Monte Carlo (MC) simulations in this work.

In addition, different incident angles of muon beams result in variations of penetration depths before reaching the SV. A test of negative muon induced SEUs on the same 65-nm bulk SRAM at an incidence angle of 45 degrees from the BS was reported in [14]. In this work, we also perform simulations with different incidence angles to see how the incident angles influence the muon induced SEUs because the muon flux on the ground is known to have a zenith angle distribution. Moreover, it is of interest to estimate SERs on the ground by considering the incident angle dependence of muon-induced SEUs and compare the result with approximately estimated SERs using the measured SEU data by conventional irradiation tests in which a device board is placed perpendicular to the incident beam.

The content of this paper is as follows. Section II introduces the setup of the irradiation tests, and Section III presents

the simulation method. Section IV reports the experimental and simulation results of positive and negative muon induced SEU cross sections with two different irradiation sides. Then, analyses and illustrations about the impact of irradiation sides and incident angles on the muon induced SEU cross section are given. Section V discusses the SER estimation on the ground with different irradiation sides and a more realistic estimation method. Finally, Section VI briefly summarizes the main results.

## II. IRRADIATION TEST

Irradiation tests with negative and positive muons were performed for 65-nm bulk SRAMs using the D2 experimental area at the J-PARC Muon Facility, MUSE. Details of the experimental procedure are reported in [6], [7].

The experimental layout is schematically illustrated in Fig. 1. The device board was placed perpendicular to the beam direction and irradiated on the PS and BS sides. It should be noted that only the experimental results of BS irradiation were reported in the previous paper [6]. Four by four SRAM chips were mounted on the device board. Each SRAM chip was fabricated in 65-nm bulk CMOS technology and has 12 Mbit memory cells. The chips are packaged in ellipsoidal resin and fixed on the device board. During the tests, only 3 by 4 chips were irradiated by muons passing through a 50 mm × 50 mm square-shaped lead collimator between the beam exit and the device board. The other four chips served as a reference, confirming that the effect of background radiations on SEU was negligible [6].

We measured the SEU cross sections of 65-nm bulk SRAM at a supply voltage of 0.5 V. Through preliminary simulations prior to testing, we selected a specific momentum range where muons stop within the chip. The momentum range at the beam exit was 24 to 36 MeV/c for PS irradiation and 34 to 42 MeV/c for BS irradiation. The muon beam is not mono-energetic, and the momentum distribution can be approximated as a normal distribution with about 5% standard deviation.

The irradiation test is regarded as a static test, and the measurement procedure is as follows. At first, all the memories were initialized by data "0". Then, the memories were in hold operation under operation voltage. After irradiation time, the data in the memories were read, and the number of SEUs was recorded. Finally, the SEU cross section  $\sigma_{<SEU>}$  was derived by

$$\sigma_{<SEU>} [\text{cm}^2/\text{Mbit}] = \frac{N_{SEU}}{\Phi [\text{cm}^{-2}] N_{bit} [\text{Mbit}]}, \quad (1)$$

where  $N_{SEU}$  is the total recorded SEUs of twelve irradiated SRAMs in the tests,  $N_{bit}$  is the total memory bits of the irradiated SRAMs with a unit of Mbit,  $\Phi$  is the fluence of incident muons during the tests which was obtained using the intensity of the pulsed muon beam. Note that the beam intensity was measured by different methods in PS and BS irradiation tests.

The relative muon intensity was measured by a beam profile monitor [15] in momentum steps of 2 MeV/c under both the PS and BS irradiations. The measurement method is outlined in the Appendix. In the BS irradiation [6], we employed a

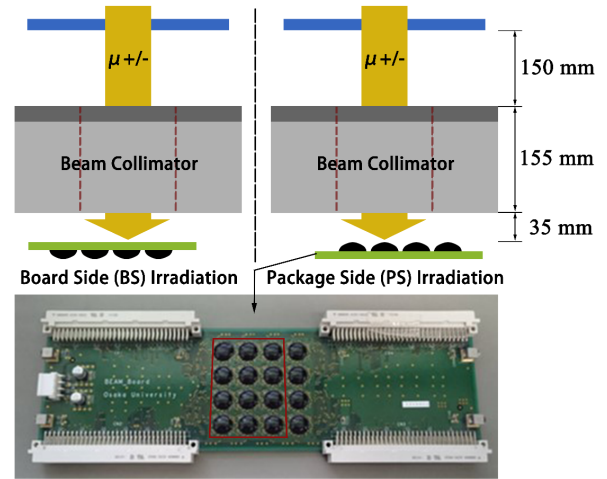


Fig. 1. Overall layout of the experimental setup and photograph of the device board under test. The irradiated chips are noted by the red frame.

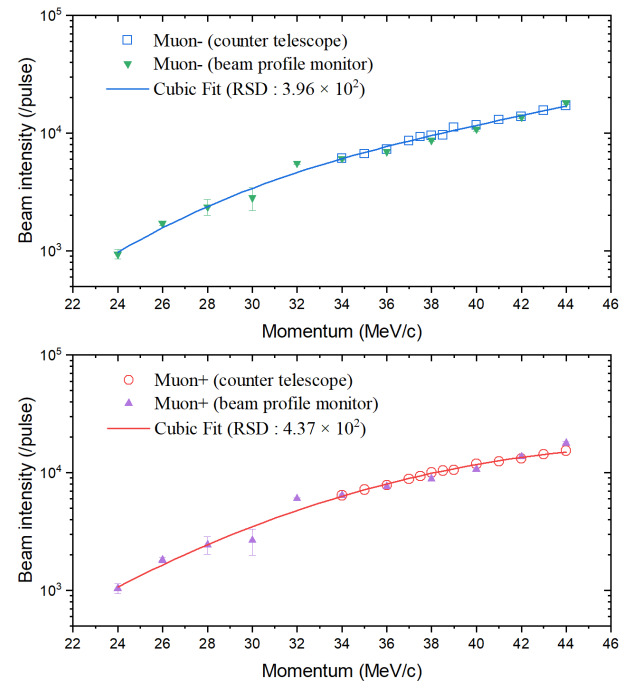


Fig. 2. Comparison of the measured intensities of the pulsed muon beams with the two different methods. The cubic fitting curves based on the measured data are also given. The upper and lower panels show the positive and negative muon intensity, respectively.

counter telescope consisting of two plastic scintillators that detect the decay electrons/positrons. The measured data with the counter telescope determined the absolute muon intensity. The detailed method can be found in [7]. The relative intensity measured with the beam profile monitor was normalized to the absolute intensity measured with the counter telescope at 34 MeV/c. As shown in Fig. 2, both the muon intensities agree well in the momentum region above 34 MeV/c. The measured data from the beam profile monitor were fitted by a cubic function over the momentum range of 24 to 44 MeV/c. The results are shown in Fig. 2. Finally, the muon intensities from

24 MeV/c to 36 MeV/c under PS irradiation were obtained by fitting the curves.

### III. MONTE CARLO SIMULATION

The Monte Carlo simulation of positive and negative muon induced SEUs in 65-nm bulk SRAMs was performed using Geant4 [16]. Direct ionization and multiple scattering of charged particles are handled by the physics list “EM Opt4”. The decay process of positive muons is implemented by “G4MuonDecayChannel”, while that of negative muons is implemented by “G4MuonMinusBoundDecay”. In addition, a pre-compound model [17] was used to simulate the negative muon capture by “G4MuMinusCapturePrecompound”, because secondary ions produced from negative muon capture have a significant impact on SEU [18].

The geometric model of the SRAM chip is shown in Fig. 3. The thickness and the composition of each layer are given in [19]. The center depth of the ellipsoidal package is about 0.935 mm. The total thickness of the device board is 1.6 mm. 12 Mbit memory cells are evenly arranged in the sensitive layer, and the sensitive volume (SV) thickness is set to 0.4  $\mu\text{m}$ . A 2.8-cm square surface muon source is placed 340 mm from the top side of the encapsulated device for both PS and BS irradiation.

For each momentum point, the beam has a Gaussian energy distribution. The standard deviation in energy was reported to average 6.4% [11] and 9.6% [6] for different momentum ranges. Since the energy distributions were not measured under the tests, the beam energy deviations in the simulation were finally decided to be 7.8% for all momentum points.

The produced charges within a SV are considered fully collected in the simulation. Thus, a SEU occurs when an incident muon deposits sufficient energy in SV greater than the threshold value  $E_{th}$ , obtained from the critical charge  $Q_c$  by:

$$E_{th} [\text{MeV}] = \frac{E_{pair} Q_c}{e} = \frac{Q_c [\text{fC}]}{44.5} \quad (2)$$

where  $e$  represents the elementary charge, and  $E_{pair}$  refers to the minimum energy to create an electron-hole pair in silicon and is equal to 3.6 eV.

### IV. RESULT AND ANALYSIS

#### A. Results of irradiation tests

In Fig. 4, the experimental results of positive and negative muon-induced SEU cross sections for 65-nm bulk SRAMs with PS and BS irradiations are plotted as a function of momentum with colored symbols. The errors bars ( $\delta_\sigma$ ) is given by considering the statistical errors in the measured flux consider the statistical errors of the measured flux ( $\Phi$ ) and the number of recorded SEU events ( $N_{SEU}$ ) in (1), using the error propagation formula:

$$\delta_\sigma = \sigma_{\langle SEU \rangle} \sqrt{\frac{1}{N_{SEU}} + \frac{\delta_\Phi^2}{\Phi^2}}, \quad (3)$$

where  $\delta_\Phi$  is the error of the average muon fluence.

Both the SEU cross sections show a broad peak structure. The peak cross section for negative muons is about 9 times

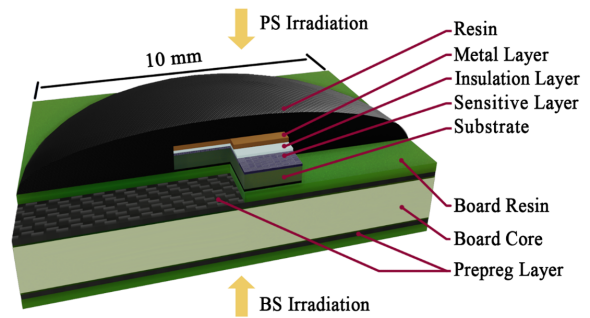


Fig. 3. Geometric model of the SRAM in simulation.

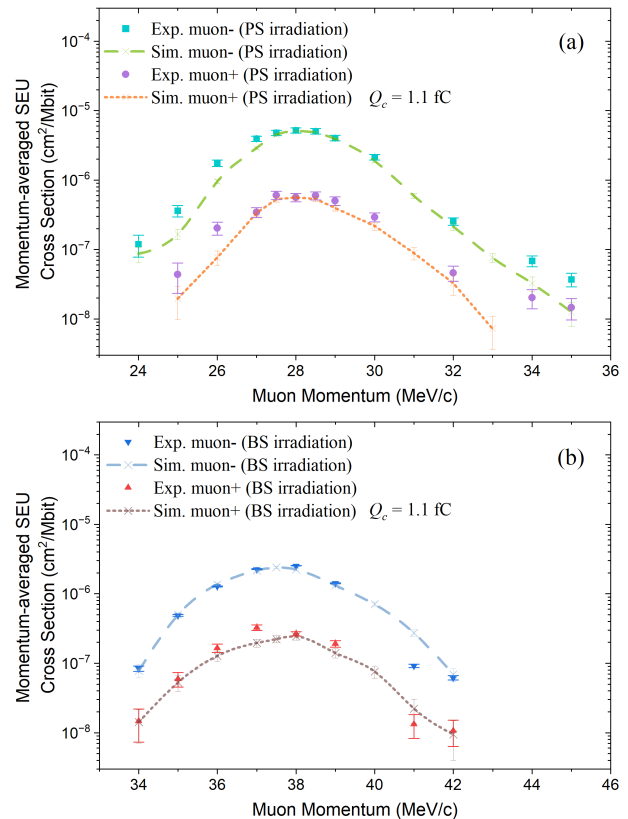


Fig. 4. Panel (a) shows the measured and simulated positive and negative muon SEU cross sections of 65-nm bulk SRAM for the PS irradiation test, while panel (b) shows those for the BS irradiation test. The measured results are shown with the colored points, while the simulated results are with colored dash curves.

larger than that for positive muons in both the PS and BS irradiations. The nuclear capture process by negative muons makes SEUs more significant than positive muons. The difference of SEUs between positive and negative muons is discussed in the previous papers [6], [7], [18].

The peak position of the BS irradiation tests is at 38 MeV/c, which is much higher than that of the PS irradiation tests, i.e., 28 MeV/c. According to [6], [7], [18], the SEU peaks of negative and positive muons appear near the end of the track due to the muon capture and the Bragg peak, respectively. Thus, the different SEU peak positions can be explained by different penetration depths. Note that the total thickness of

the device board (1.6 mm) and substrate (0.3 mm) is much larger than the thickness of the package resin (0.935 mm).

Moreover, the peak SEU cross section of the PS irradiation is about twice larger than that of the BS irradiation. The ratios of the peak SEU cross sections for the PS and BS irradiations are given by

$$k_{CS-} = \frac{\sigma_{p-}}{\sigma_{b-}} = 2.06 \pm 0.18, \quad (4)$$

$$k_{CS+} = \frac{\sigma_{p+}}{\sigma_{b+}} = 2.13 \pm 0.33, \quad (5)$$

for negative and positive muons, respectively. In (4) and (5),  $\sigma_{p-}$  and  $\sigma_{b-}$  denote the peak SEU cross section for negative muon PS and BS irradiation, respectively. Similarly,  $\sigma_{p+}$  and  $\sigma_{b+}$  represent the peak SEU cross sections for positive muon PS and BS irradiations, respectively.

### B. Results of Simulation

The simulation results of momentum dependent SEU cross sections for both PS and BS irradiation tests are presented by the dash curves and compared with the experimental results in Fig. 4. The critical charge  $Q_c$  was determined to be 1.1 fC in simulations so that the simulated SEU cross sections reproduce the experiment well in both PS and BS irradiation tests.

From Fig. 4, the simulated peak positions and cross-sections under the BS irradiation agree well with the experimental results for both positive and negative muons. As for the PS irradiation, the simulated results of the peak position and the cross sections near the peak region agree with the experimental results. However, the simulated cross-sections are smaller than the experimental ones in the non-peak area, especially in the high-momentum region. No SEU was observed in the simulation for the 34 and 35 MeV/c positive muons. This may be because the momentum distribution of incident muons is not strictly Gaussian and has tails in the low and high momentum regions. In addition, modeling errors in the ellipsoidal shape of the package, especially the surface curvature, may also influence the simulation result in the non-peak region under PS irradiation tests.

### C. Impact of irradiation side on SEU cross-section

We performed a simulation-based analysis to understand why the magnitude of peaked SEU cross-sections differs by approximately twice between the PS and BS irradiations in addition to the difference in the peak momentum position.

For positive muons, the difference in peak positions between the PS and BS irradiations can be easily explained by the difference in penetration depths before muons reach the SV, because the SEU cross section is maximized at the momentum where the Bragg peak is located in the SV.

Next, the ratio  $k_{CS+}$  in (4) can be quantitatively explained with a concept of "effective SEU fluence," which was defined and obtained by approximate calculation in [20] to investigate the impact of energy straggling on SEUs. The deposition energy in the SV to cause SEUs has a threshold value ( $E_{th}$ ), and the deposition energy of positive muons depends on

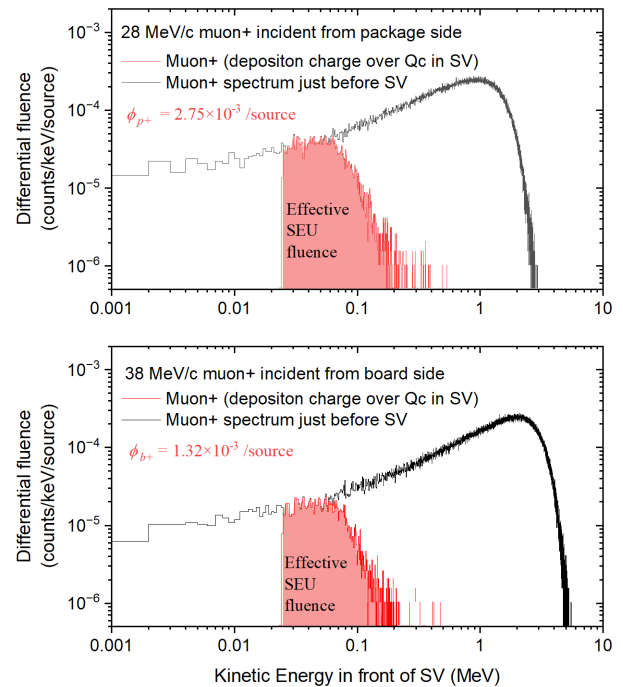


Fig. 5. Energy distributions of positive muons before entering the SV with different irradiation sides are shown with black curves. The lower panel shows the BS irradiation case, while the upper panel shows the PS irradiation case. The red curves mean the positive muons with deposition energy over  $E_{th}$  in SV. The integrated values of red curves are defined as "effective SEU fluences," marked with  $\phi_{b+}$  for the BS case and  $\phi_{p+}$  for the PS case.

their kinetic energy before entering the SV. Due to stochastic processes such as energy straggling and multiple scattering in device materials, the kinetic energy of positive muons just before the SV has a distribution even for mono-energetic muons. Using simulation, the energy spectrum of positive muons was calculated just before the SV for 28 MeV/c PS irradiation and 38 MeV/c BS irradiation. The results are shown with the black curves in the upper and lower panels in Fig. 5. The red curves indicate the energy spectrum of positive muons with energy deposition over  $E_{th}$  in SV, and the integrated values of the red curves are defined as "effective SEU fluence." This means the relative fluence of muons that effectively induce SEUs.

In Fig. 5, the effective SEU fluences for PS irradiation with 28-MeV/c positive muons and BS irradiation with 38-MeV/c positive muons are given by  $\phi_{p+}$  and  $\phi_{b+}$ , respectively. They differ from each other because the muon energy distributions before the SV are different between PS and BS irradiations due to the change in the incident depth. Their ratio  $k_{EF+}$  is obtained by

$$k_{EF+} = \frac{\phi_{p+}}{\phi_{b+}} = 2.08 \pm 0.03, \quad (6)$$

where the error is estimated from the statistical error of the simulated effective SEU fluence.

As shown in Fig. 6, the  $k_{CS+}$  value in (4) and the  $k_{EF+}$  value in (6) agree within their error margin. Thus, the effective SEU fluence is essential to understand that the magnitude of

the peak SEU cross-sections is different by a factor of about two between the PS and BS irradiations with positive muons.

For negative muons, the main contribution of the SEUs is the secondaries released by the muon capture reaction. Therefore, the spatial distribution of the negative muon capture events inside the device is counted by simulation and shown with the black curves in Fig. 7. The vertical axis is the differential events number per incidence length, and the horizontal axis is the position of the events described by the distance from the bottom of the package. The device structure in the position of an event is marked on the top of the figure. The upper panel shows the case of PS irradiation with 28-MeV/c negative muons, and the lower panel shows the case of BS irradiation with 38-MeV/c negative muons. Note that the peak of muon capture events appears in the metal layer, and the difference between muon capture events in the package and those in the SRAM chip is due to different materials.

Once the secondary ions released from the muon capture reaction deposit the energy over  $E_{th}$  in the SV, the events are counted at their released (initial) position, shown with curves of different colors for different secondary ions in Fig. 7. The green curves represent the hydrogens (H) including protons, deuterons, and tritons. The blue curves represent the alpha particles (He), and the purple ones represent the heavy ions (HI), like aluminum, magnesium, and sodium. Contributions from HI are distributed closest to the SV, followed by alpha, and those from hydrogens are distributed furthest. Their different ranges in the device material can explain this trend. Fig. 7 shows that distributions of muon capture events and their released secondary ions differ between the PS and BS irradiations due to the changing incidence depth in different irradiation sides.

Then, we add the events of all the secondary ions and negative muons (direct ionization) whose deposition energies in the SV are over  $E_{th}$  and define it as the effective SEU fluence of negative muons. The effective SEU fluences for PS irradiation with negative muons of 28 MeV/c and BS irradiation with negative muons of 38 MeV/c are denoted by  $\phi_{p-}$  and  $\phi_{b-}$ , respectively. Their ratio  $k_{EF-}$  is defined and calculated by

$$k_{EF-} = \frac{\phi_{p-}}{\phi_{b-}} = 1.97 \pm 0.04. \quad (7)$$

Figure 6 also shows the comparison between  $k_{EF-}$  and  $k_{CS-}$ . Despite the minor differences within the error margin,  $k_{EF-}$  and  $k_{CS-}$  agree well. The effective SEU fluence of the negative muon can effectively explain the measured ratio of the peak SEU cross sections between PS and BS irradiations.

#### D. Incident angle dependence of SEU cross sections.

In the previous paper [14], the same 65-nm bulk SRAM chips were tested against negative muon BS irradiation, all of which were oriented in the same tilted direction. At that time, the short axis of the device board, i.e., the Bit line (BL) direction of the SRAM, was tilted at 45 degrees with respect to normal incidence, as shown in the inset of Fig. 8. The shift of the peak position of the SEU cross section relative to the vertical incidence was reported. We calculated the SEU

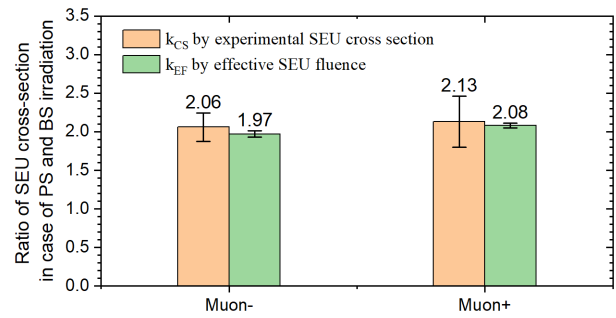


Fig. 6. Comparison of the experimental and estimated ratios of peak cross sections for PS irradiation to those for BS irradiation for both positive and negative muons.

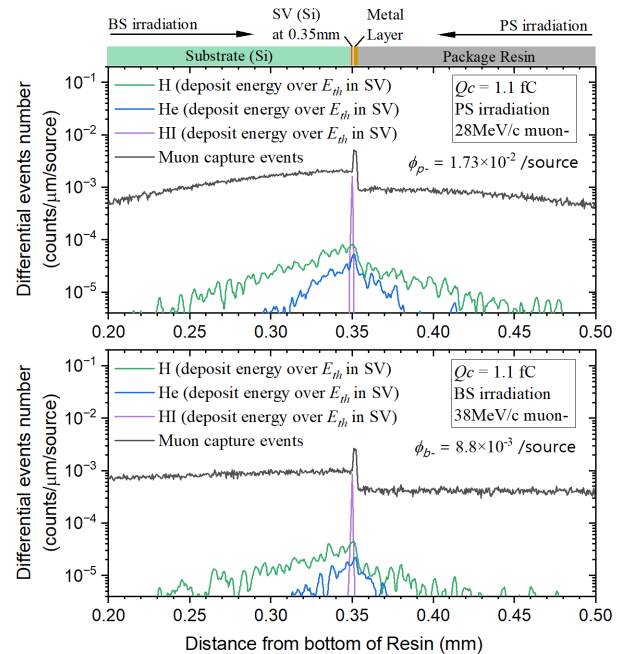


Fig. 7. Spatial distributions of muon capture events inside the 65-nm bulk SRAM for PS irradiation with 28-MeV/c negative muons and BS irradiation with 38-MeV/c negative muons. The events of their released secondaries depositing energy over  $E_{th}$  in SV are also shown with colored curves.

cross sections as a function of incident momentum using the simulation method with Geant4 described in Sec. III. The result is compared with the normalized experimental data in Fig. 8 since only the normalized cross section is given experimentally. The simulated peak position is consistent with the experimental result, and the normalized cross-sections also agree with the experimental one. Thus, it was found that this simulation method can also be applied when muons are irradiated obliquely.

We then performed further simulations for a wide range of angles to investigate the effect of incident angle on the SEU cross section. The result is shown in Fig. 9. The rotation angle of the device board on the x-axis is marked with  $\theta$ , equal to the incident angle. Since the penetration depth of the negative muons before reaching the SV increases with  $\theta$ , the peak position of simulated SEU cross sections moves toward higher momenta. On the other hand, the energy straggling and

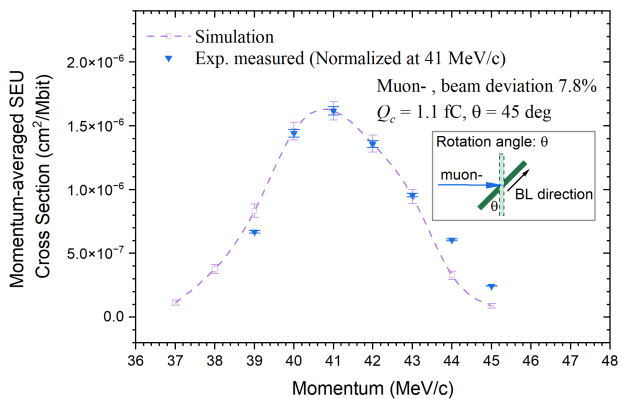


Fig. 8. Comparison of simulated SEU cross-sections for a 45-degree negative muon incident from the board side with normalized experimental data. The measured values in irradiation tests are taken from [14] and normalized to the simulation results at 41 MeV/c.

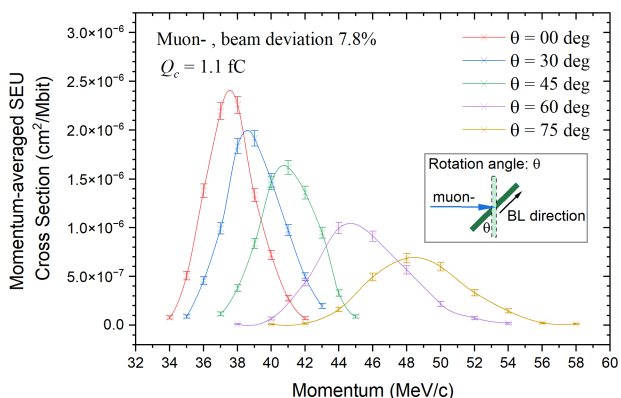


Fig. 9. Simulation results of the momentum-dependent SEU cross sections for negative muon incident from the board side at different incidence angles.

multiple scattering become more pronounced with increasing penetration depth, resulting in a lower effective SEU fluence. This reduces the peak cross-section.

## V. DISCUSSION

In this section, muon-induced SERs under a terrestrial environment are estimated based on the results of previous Section IV, and the effect of zenith angle distribution of terrestrial muon flux on SERs is discussed.

### A. SER estimation based on the muon irradiation of which beam direction is vertical to the device

The SER under a terrestrial environment can be estimated by the following equation:

$$SER = \int_0^{\infty} \varphi(E) \sigma(E) dE, \quad (8)$$

where  $\varphi(E)$  represents the flux of muons within the energy range  $[E, E+dE]$  in a specific terrestrial environment, and  $\sigma(E)$  is the SEU cross section as a function of kinetic energy  $E$ .

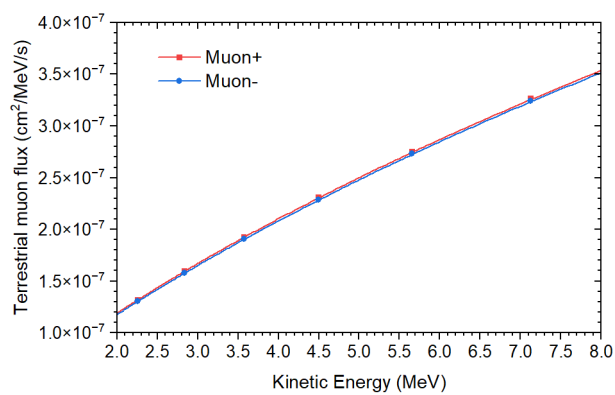


Fig. 10. Fluxes of positive and negative muons within the energy range that is sensitive to inducing SEU in the 65-nm bulk SRAMs at sea level in Tokyo. The result is calculated by using EXPACS [21].

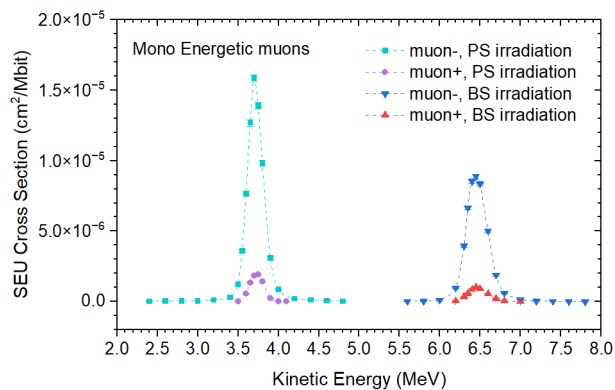


Fig. 11. Kinetic energy dependent SEU cross sections induced by mono-energetic positive and negative muons in 65-nm bulk SRAM with PS and BS irradiations. The results are derived from Geant4 simulations.

We estimated the SER for the 65-nm bulk SRAM. The fluxes of terrestrial positive and negative muons were calculated by the EXPACS tool employing a PHITS-based analytical radiation model (PARMA) [21]. In Fig. 10, the fluxes derived from the EXPACS calculation are shown in the energy range that is sensitive to inducing SEUs in the 65-nm SRAM device of interest. The fluxes of positive and negative muons are very close and increase with increasing kinetic energy. We assume that mono-energetic muons are incident to the device in the vertical direction. The simulated SEU cross sections,  $\sigma(E)$  in (8), are plotted for both PS and BS irradiations in Fig. 11. Since no SEU events are observed for muons beyond the energy range shown in Fig. 11, the  $\sigma(E)$  is assumed to be zero in SER calculations. The estimated SERs for positive and negative muons are shown in Fig. 12. The unit of SER is FIT/Mbit where FIT means Fault in Time, i.e., the number of SEU occurrences per  $10^9$  h. For both positive and negative muons, the estimated SERs for the BS irradiation are slightly larger than those for the PS irradiation. The difference is at most 21%. In this case, the impact of the irradiation side on SER prediction is relatively weak.

This weak dependency can be understood as follows. The SV is at a deeper depth in the BS irradiation case than in the PS irradiation case. As a result, the peak position of SEU

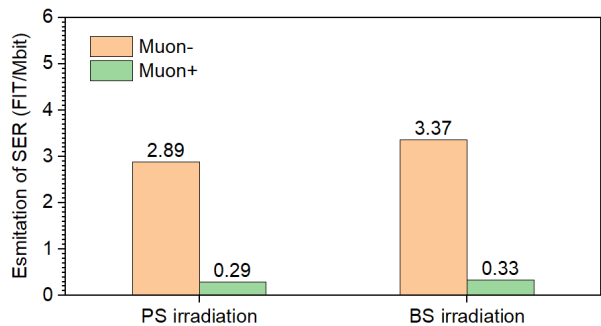


Fig. 12. The estimated SERs of positive and negative muons for 65-nm bulk SRAM. The SEU cross-sections derived from the PS and BS irradiation tests are used in the estimation.

cross sections shifts to higher kinetic energy, resulting in larger  $\varphi(E)$  in (8). On the other hand, the energy straggling and multiple scattering is more considerable because the muon penetration path to SV is longer in the BS irradiation case, resulting in a smaller peak cross-section, i.e., a smaller  $\sigma(E)$  in (8) as shown in Fig. 11. Finally, the SERs defined by (8) are similar between PS and BS irradiations.

### B. Realistic SER estimation considering the zenith angle distribution of muon flux in terrestrial environment

Since the muon flux on the ground has a zenith angle distribution, the muon incident angle is expected to affect the SEU cross section of the SRAM device. Equation (8) needs to be modified so that the zenith angle distribution of the muon flux can be considered as follows:

$$\text{SER} = 2\pi \iint \varphi(E, \theta) \sigma(E, \theta) \sin(\theta) dE d\theta, \quad (9)$$

where  $\varphi(E, \theta)$  represents the muon differential flux with zenith angle  $\theta$  in the energy range  $[E, E + dE]$ , and  $\sigma(E, \theta)$  denotes the muon SEU cross sections as a function of kinetic energy and zenith angle. The numerical integration in (9) was performed using an angular distribution calculated at 15-degree intervals.

Figure 13 shows the calculated zenith angle distribution of negative muon flux at sea level by EXPACS [21]. The simulation-derived SEU cross-sections of mono-energetic negative muons for the 65-nm bulk SRAM are shown with different incident angles for both PS and BS irradiations in Fig. 14. Finally, Fig. 15 compares the SER estimated by (9) with the SER for the perpendicular incidence estimated in Sec. V-A. Both results are almost the same.

As reported in [8], the estimated muon SER is much lower than the neutron SER of the same 65-nm bulk SRAMs. Therefore, our results on the zenith angle dependence of 65 nm SRAM are expected to have little impact on the estimation of total SERs on the ground. However, the contribution of muons to the total SERs is predicted to be more significant in devices with smaller technology [4]. Thus, further investigation is required to confirm whether the angular distribution of muons on the ground affects the SER estimations for devices with smaller technologies.

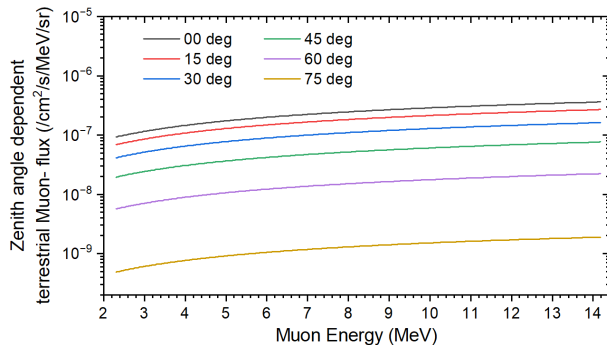


Fig. 13. Differential fluxes of negative muons with zenith angle  $\theta$  within the energy range that is sensitive to inducing SEU in the 65-nm bulk SRAMs at sea level in Tokyo. The result is calculated by using the EXPACS [21].

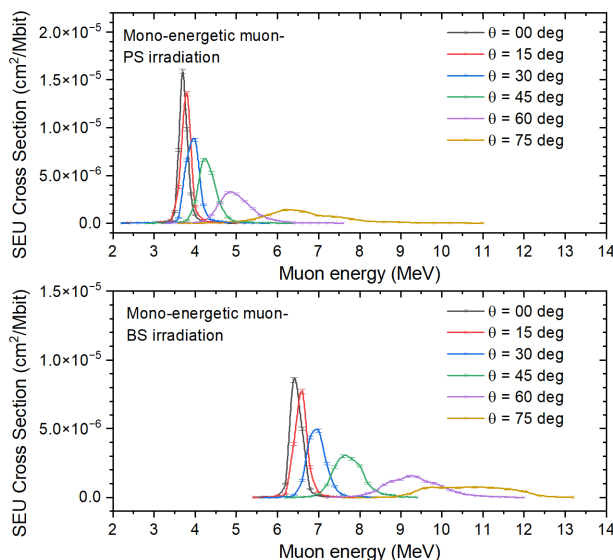


Fig. 14. Mono-energetic negative muons induced SEU cross sections in 65-nm bulk SRAM with different incident angles in PS and BS irradiation.

## VI. CONCLUSION

Negative and positive muon irradiation tests of 65 nm bulk SRAMs were performed with two different irradiation sides: package side (PS) and board side (BS). The results of the PS irradiation tests were newly analyzed and compared with those of the previous BS irradiation tests. We found that the peak SEU cross section is at 28 MeV/c for PS irradiation, which is not the same as 38 MeV/c for BS irradiation. The magnitude of the peak SEU cross section for PS irradiation is approximately twice that of BS irradiation for both positive and negative muons. The simulated SEU cross sections with Geant4 agree well with the measured ones for both PS and BS irradiation tests, except in the non-peak momentum region under PS irradiation.

Next, the concept of effective SEU fluence was introduced to explain quantitatively the impact of irradiation side on the SEU cross section. It was found that the measured ratios of the peak SEU cross section for PS and BS irradiations, i.e., about two, are consistent with the ratios calculated from the effective fluence within the margin of error. From the analyses

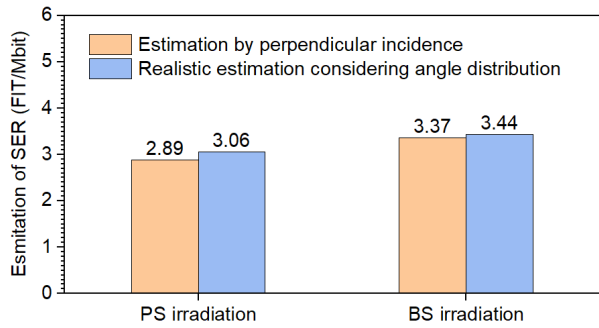


Fig. 15. Realistic SER estimation of negative muons in 65-nm bulk SRAM considering the zenith angle distribution of muon flux in the terrestrial environment are compared with the approximate SER estimation derived from the perpendicular incidence.

with the effective SEU fluence, we revealed that the difference in observed SEU cross sections between PS and BS irradiation is caused by the differences in energy straggling and multiple scattering due to changes in penetration depth depending on the incident direction. We investigated the dependence of the incident angle of muons on the SEU cross-section. As a result, the incident angle affected the momentum and the magnitude when the SEU cross section formed the peak. This can also be explained by the variation of penetration depth depending on the incident angle.

Based on the above results, we estimated the terrestrial muon induced SERs for the same 65-nm bulk SRAMs using the simulated SEU cross sections and the muon fluxes calculated by EXPACS. For both positive and negative muons, the estimated SERs for BS irradiation in the direction perpendicular to the device board are slightly larger than those for PS irradiation. However, the difference was at most 21%. Thus, the impact of the irradiation side on SER prediction was found to be relatively weak.

Finally, we predicted the SERs under a more realistic environment by considering the zenith angle distribution of muon flux. As a result, the predicted SER was found to have no significant difference from that without zenith angle distribution. Therefore, experimental data from conventional irradiation tests in which a device board is placed perpendicular to the incident beam are expected to be useful in estimating muon-induced SERs on the ground.

#### APPENDIX

The relative muon beam intensity was measured using a beam profile monitor [15] for both the PS and BS irradiation tests. The monitor consists of a scintillation screen and UVT acrylic blocks contained in a light-tight polyvinyl chloride (PVC) tube for light shielding. A round-shaped scintillation screen (130 mm in diameter and 2 mm thick) was made of an EJ-212 plastic scintillator. When muons interact with the scintillator, the scintillation light is generated from the deposited energy. A two-dimensional muon beam profile can be measured as a CCD camera image. The device board was removed during the beam profile measurement, and the profile monitor was placed behind the beam collimator. The muon beam profiles were measured at several incident momenta.

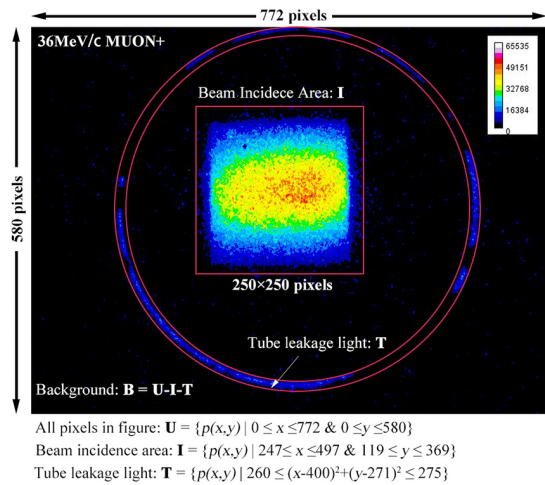


Fig. A-1. A two-dimensional profile image of the beam intensity for a positive muon beam of 36 MeV/c.

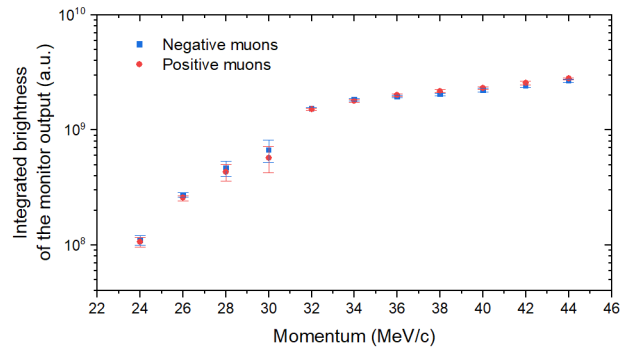


Fig. A-2. Integrated brightness  $L$  of the output images of beam profile monitor as a function of momentum.

In Fig. A-1, a measured two-dimensional profile image of the beam intensity is shown for a positive muon beam of 36 MeV/c. The beam intensity increases toward the center, shaped like a square, due to the beam collimator slit. The brightness values in the integration area (region **I** in Fig. A-1) were integrated after background noise subtraction. The bright pixels in the ring area marked with **T** come from the leakage lights in the connection position between the light transport tube and the CCD camera lens.

Brightness integration was performed on the monitor output images from 24 to 44 MeV/c in steps of 2 MeV/c. The results are shown in Fig. A-2.

The integrated brightness  $L$  in Fig. A-2 is proportional to the number of generated photons in the scintillator. To convert  $L$  to the relative beam intensity, the non-linear response of organic scintillators (the Birks effect [22], [23]) should be considered. The number of generated photons in the scintillator per incident muon, i.e.,  $N_{ph}$ , can be expressed by

$$N_{ph} = \int_0^d \frac{Y_0 \frac{dE}{dx}}{1 + kB \frac{dE}{dx}} dx, \quad (10)$$

where  $kB$  is the Birks constant,  $d$  is the scintillator thickness,  $dE/dx$  is the ionization density, and  $Y_0$  is the absolute light

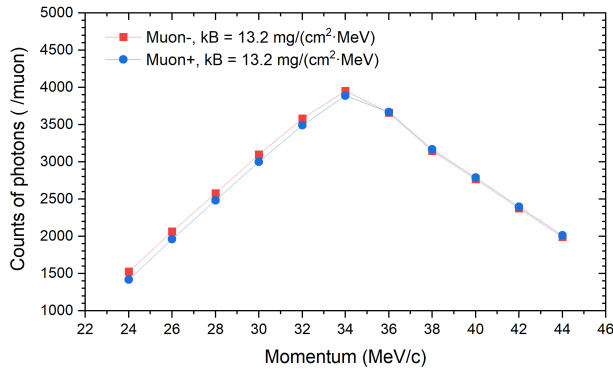


Fig. A-3. Simulated photon productions  $N_{ph}$  in the scintillator for incident muons with different momenta.

yield, which is 10050 photons/MeV for EJ-212 scintillator according to [24].

The photon productions of the EJ-212 plastic scintillator for muons with different momenta were simulated by Geant4. The ionization densities  $dE/dx$  of muons were evaluated over the momentum range shown in Fig. A-2, and  $kB$  was set to  $13.2 \text{ mg}/(\text{cm}^2 \cdot \text{MeV})$  from [23]. The results for positive and negative muons are shown in Fig. A-3. The slope of the curve is changed at 34 MeV/c because the muons above 34 MeV/c pass through the scintillator, and the deposited energy decreases with increasing momentum. In the scintillator, some negative muons are stopped and release secondary ions by muon capture when their momentum is below 34 MeV/c. This leads to a slightly larger average deposition energy and photon productions compared to positive muons, as shown in Fig. A-3.

Finally, the relative beam intensity shown in Fig. 2 was obtained using

$$I_{rel}(p_\mu) = \frac{L(p_\mu)}{N_{ph}(p_\mu)}, \quad (11)$$

where  $p_\mu$  is the momentum of the muon,  $L$  is the integrated brightness in Fig. A-2, and  $N_{ph}$  is the number of photon production per muon in Fig. A-3.

#### ACKNOWLEDGMENT

The muon irradiation tests were performed at the Materials and Life Science Experimental Facility of the J-PARC under user programs Nos. 2016B0046 and 2017A0139.

#### REFERENCES

- [1] B. D. Sierawski *et al.*, "Muon-induced single event upsets in deep-submicron technology," *IEEE Trans. Nucl. Sci.*, vol. 57, no. 6, pp. 3273–3278, Dec. 2010, doi: 10.1109/TNS.2010.2080689.
- [2] B. D. Sierawski *et al.*, "Effects of scaling on muon-induced soft errors," in *Proc. Int. Rel. Phys. Symp.*, Monterey, CA, USA, Apr. 2011, pp. 3C.3.1–3C.3.6, doi: 10.1109/IRPS.2011.5784484.
- [3] B. D. Sierawski *et al.*, "Bias dependence of muon-induced single event upsets in 28 nm static random access memories," in *Proc. Int. Rel. Phys. Symp.*, Waikoloa, HI, USA, Jun. 2014, pp. 2B.2.1–2B.2.5, doi: 10.1109/IRPS.2014.6860585.
- [4] G. Hubert, L. Artola, and D. Regis, "Impact of scaling on the soft error sensitivity of bulk, FDSOI and FinFET technologies due to atmospheric radiation," *Integration*, vol. 50, pp. 39–47, Jun. 2015, doi: 10.1016/j.vlsi.2015.01.003.

- [5] J. M. Trippe *et al.*, "Predicting muon-induced SEU rates for a 28-nm SRAM using protons and heavy ions to calibrate the sensitive volume model," *IEEE Trans. Nucl. Sci.*, vol. 65, no. 2, pp. 712–718, Feb. 2018, doi: 10.1109/TNS.2017.2786585.
- [6] W. Liao *et al.*, "Measurement and mechanism investigation of negative and positive muon-induced upsets in 65-nm bulk SRAMs," *IEEE Trans. Nucl. Sci.*, vol. 65, no. 8, pp. 1734–1741, Aug. 2018, doi:10.1109/TNS.2018.2825469.
- [7] S. Manabe *et al.*, "Negative and positive muon-induced single event upsets in 65-nm UTBB SOI SRAMs," *IEEE Trans. Nucl. Sci.*, vol. 65, no. 8, pp. 1742–1749, Aug. 2018, doi: 10.1109/TNS.2018.2839704.
- [8] S. Manabe, Y. Watanabe, W. Liao, M. Hashimoto, and S. Abe, "Estimation of muon-induced SEU rates for 65-nm bulk and UTBB-SOI SRAMs," *IEEE Trans. Nucl. Sci.*, vol. 66, no. 7, pp. 1398–1403, Jul. 2019, doi: 10.1109/TNS.2019.2916191.
- [9] T. Mahara *et al.*, "Irradiation test of 65-nm bulk SRAMs with DC muon beam at RCNP-MuSIC facility," *IEEE Trans. Nucl. Sci.*, vol. 67, no. 7, pp. 1555–1559, Jul. 2020, doi: 10.1109/TNS.2020.2972022.
- [10] T. Kato *et al.*, "Muon-induced single-event upsets in 20-nm SRAMs: comparative characterization with neutrons and alpha particles," *IEEE Trans. Nucl. Sci.*, vol. 68, no. 7, pp. 1436–1444, Jul. 2021, doi: 10/gnk4st.
- [11] Y. Miyake *et al.*, "J-PARC muon source, MUSE," *Nucl. Instrum. Methods Phys. Res. Sect. Accel. Spectrometers Detect. Assoc. Equip.*, vol. 600, no. 1, pp. 22–24, Feb. 2009, doi: 10.1016/j.nima.2008.11.016.
- [12] Y. Miyake *et al.*, "Current status of the J-PARC muon facility, MUSE," *J. Phys. Conf. Ser.*, vol. 551, no. 1, Dec. 2014, Art. no. 012061, doi: 10.1088/1742-6596/551/1/012061.
- [13] S. Abe, W. Liao, S. Manabe, T. Sato, M. Hashimoto, and Y. Watanabe, "Impact of irradiation side on neutron-induced single-event upsets in 65-nm bulk SRAMs," *IEEE Trans. Nucl. Sci.*, vol. 66, no. 7, pp. 1374–1380, Jul. 2019, doi: 10.1109/TNS.2019.2902176.
- [14] W. Liao *et al.*, "Impact of the angle of incidence on negative muon-induced SEU cross sections of 65-nm bulk and FDSOI SRAMs," *IEEE Trans. Nucl. Sci.*, vol. 67, no. 7, pp. 1566–1572, Jul. 2020, doi: 10.1109/TNS.2020.2976125.
- [15] T. U. Ito, A. Toyoda, W. Higemoto, M. Tajima, Y. Matsuda, and K. Shimomura, "Online full two-dimensional imaging of pulsed muon beams at J-PARC MUSE using a gated image intensifier," *Nucl. Instrum. Methods Phys. Res. Sect. Accel. Spectrometers Detect. Assoc. Equip.*, vol. 754, pp. 1–9, Aug. 2014, doi: 10.1016/j.nima.2014.04.014.
- [16] S. Agostinelli *et al.*, "Geant4—a simulation toolkit," *Nucl. Instrum. Methods Phys. Res. Sect. Accel. Spectrometers Detect. Assoc. Equip.*, vol. 506, no. 3, pp. 250–303, Jul. 2003, doi: 10.1016/S0168-9002(03)01368-8.
- [17] K. K. Gudima, S. G. Mashnik, and V. D. Toneev, "Cascade-exciton model of nuclear reactions," *Nucl. Phys. A*, vol. 401, no. 2, pp. 329–361, Jun. 1983, doi: 10.1016/0375-9474(83)90532-8.
- [18] W. Liao *et al.*, "Negative and positive muon-induced SEU cross sections in 28-nm and 65-nm planar bulk CMOS SRAMs," in *Proc. Int. Rel. Phys. Symp.*, Monterey, CA, USA, Mar. 2019, pp. 396–400, doi: 10.1109/IRPS.2019.8720568.
- [19] S. Abe *et al.*, "A terrestrial SER estimation methodology based on simulation coupled with one-time neutron irradiation testing," *IEEE Trans. Nucl. Sci.*, vol. 70, no. 8, pp. 1652–1657, Aug. 2023, doi: 10.1109/TNS.2023.3280190.
- [20] Y. Deng and Y. Watanabe, "A method of predicting muon-induced SEUs using proton tests and Monte Carlo simulation," *IEEE Trans. Nucl. Sci.*, vol. 70, no. 8, pp. 1775–1782, Aug. 2023, doi: 10.1109/TNS.2023.3267767.
- [21] T. Sato, H. Yasuda, K. Niita, A. Endo, and L. Sihver, "Development of PARMA: PHITS-based analytical radiation model in the atmosphere," *Radiat. Res.*, vol. 170, no. 2, pp. 244–259, Aug. 2008, doi: 10.1667/RR1094.1.
- [22] J. B. Birks, "Scintillations from organic crystals: specific fluorescence and relative response to different radiations," *Proc. Phys. Soc. Sect. A*, vol. 64, no. 10, pp. 874–877, Oct. 1951, doi: 10.1088/0370-1298/64/10/303.
- [23] G. D. Badhwar, C. L. Deney, B. R. Dennis, and M. F. Kaplon, "The nonlinear response of the plastic scintillator NE102," *Nucl. Instrum. Methods*, vol. 57, pp. 116–120, Jan. 1967, doi: 10.1016/0029-554X(67)90507-1.
- [24] I. Holl, E. Lorenz, and G. Mageras, "A measurement of the light yield of common inorganic scintillators," *IEEE Trans. Nucl. Sci.*, vol. 35, no. 1, pp. 105–109, Feb. 1988, doi: 10.1109/23.12684.